Study of the rectangular cross-flow flat-sheet membrane module for desalination by vacuum membrane distillation

CrossMark

Chel-Ken Chiam*, Rosalam Sarbatly

Membrane Technology Research Group, Material and Mineral Research Unit, Faculty of Engineering, Universiti Malaysia Sabah, Jalan UMS, 88400 Kota Kinabalu, Sabah, Malaysia

A B S T R A C T

This work presents a study of the heat and mass transfer performance of desalination in a laboratory-scale rectangular cross-flow flat-sheet membrane module by vacuum membrane distillation (VMD) experiments. Results show that the traditional Nusselt and Sherwood correlations, which are frequently employed in the membrane distillation literature, are not suitably used to estimate the heat and mass transfer coefficients in the VMD system for Reynolds numbers ranging from 150 to 1400. In this study, it was observed that approximately 30% of the experimental data fit well with semi-empirical correlations whose empirical constants are $a = 2.76 \times 10^{-3}$, $b = 0.97$ and $c = 3.7909$. The heat transfer process is limited by the resistances in the feed boundary layer and the membrane. The heat transfer resistance in the membrane increases when that in the feed boundary layer decreases and vice versa. More than 50% of the heat transfer resistances occur in the liquid feed phase at feed flow rates below 1200 mL/min, whereas the remaining occur in the membrane itself. At feed flow rates that exceed 1200 mL/min, the heat transfer resistance in the membrane becomes dominant. The Knudsen-viscous resistance controls the mass transfer through the membrane while the mass transfer resistance in the liquid feed phase is absent.

© 2016 Elsevier B.V. All rights reserved.

1. Introduction

Desalination is becoming increasingly well-known as a promising alternative source of potable water. Current commercial desalination technologies include those that implement reverse osmosis (RO) and thermal evaporation. These commercial desalination technologies, however, are relatively energy-intensive, e.g. high operating pressure in RO and high operating temperature in thermal evaporation techniques. Compared to RO and thermal evaporation techniques, membrane distillation (MD) consumes less energy, that is, the process can operate with low- grade heating sources under non-pressurised conditions [1–3]. Consequently, MD has been considered a process intensification method because it is less costly and safer [4,5].

Recently, the use of MD for producing fresh water through desalination has been highly recommended [6]. In desalination by the MD process, saline water is brought into direct contact with the upstream side of a porous hydrophobic membrane, and water vapour is thermally driven through the membrane. Water vapour transport across the membrane occurs when a driving force between the upstream and the downstream sides of the membrane exists. The MD methods designed to maintain the driving force can be categorised into four types of configurations: direct contact MD (DCMD), air-gap MD (AGMD), sweeping-gas MD (SGMD) and vacuum MD (VMD). Desalination using VMD is the most frequently investigated configuration because it exhibits the highest flux amongst the abovementioned types [7,8].

Highly permeable membranes are the most suitable for use in the VMD process for desalination applications [9]. Because such membranes are porous and permeable, heat and mass transfer occur simultaneously during the separation process. Traditional Nusselt and Sherwood correlations, respectively, have been employed in most published studies of VMD as well as other MD configurations to predict the heat and mass transfer coefficients in the feed phase [10–12]. However, these correlations are developed exclusively for heat exchangers, which feature impermeable and non-porous walls. Compared to those in non-porous walls, polarisation effects are reduced in porous membranes because the total solid-liquid contact area is relatively small. As a result, the traditional Nusselt and Sherwood correlations may underestimate the heat and mass transfer coefficients. Although the applicability of the correlations has

* Corresponding author. Fax: +60 88 320348.
E-mail addresses: qiujingchiam@gmail.com, chiamchelken@ums.edu.my
(C.-K. Chiam), rslam@ums.edu.my (R. Sarbatly).

Nomenclature

a, b, c	Empirical constants for Eqs. (23)–(25)
C	Membrane distillation coefficient ($kg/m^2 s Pa$); concentration (wt%)
d or D	Diameter (m); diffusivity (m^2/s)
Gr	Grashof number
h	Heat transfer coefficient ($W/m^2 K$)
H	Overall heat transfer coefficient ($W/m^2 K$)
ΔH_V	Heat of vaporization (J/kg)
J	Mass flux ($kg/m^2 s$ or $kg/m^2 h$)
k_B	Boltzmann constant (1.38×10^{-23} J/K)
k_L	Solute mass transfer coefficient (m/s)
k_T	Thermal conductivity (W/m K)
K_m	Membrane permeability coefficient ($s\, mole^{1/2}\, m^{-1}\, kg^{-1/2}$)
Kn	Knudsen number
L	Length (m)
M	Molecular weight (kg/mol)
n	Mole fraction
n_+, n_-	Valences
Nu	Nusselt number
$\overline{P}$	Mean partial pressure (Pa)
P	Vapour pressure (Pa); pressure (Pa)
ΔP	Vapour pressure difference (Pa); pressure difference (Pa)
$P°$	Saturated vapour pressure (Pa)
Pr	Prandtl number
Q	Volumetric flow rate (mL/min); heat flux ($J/m^2 s$)
r	Radius (m)
R	Gas constant (8.31 J/mol K); resistance (Pa m^2 h/kg)
Re	Reynolds number
Sc	Schmidt number
Sh	Sherwood number
T	Temperature (K)

Subscript
b	Bulk
f	Feed
g	Gas
h	Hydraulic
I	Interface
L	Liquid
m	Membrane
p	Permeate; pore
s	Solute
v	Vapour
w	Water

Greek letters
δ	Thickness (m)
ε	Porosity
η_v	Viscosity of vapour [Pa s]
λ	Mean free path (m)
λ_+, λ_-	Limiting ionic conductance
μ	Viscosity of liquid (Pa s)
ρ	Density (kg/m^3)
σ	Collisions diameter (m)
τ	Tortuosity
γ	Activity coefficient

been questioned over the past decade [13–15], studies on the re-evaluation of the correlations are still limited. Additionally, the developed correlations were validated by using pure water rather than applied to aqueous solutions [14,15].

In this work, a laboratory-produced rectangular cross-flow flat-sheet membrane module is studied for desalination process. NaCl solutions are examined as the feed solutions in which polarisation effects and transport resistances are considered. The semi-empirical correlation that is formulated especially for the rectangular cross-flow flat-sheet membrane module and pure water as the feed solution in our previous paper [16] is investigated in this study. The fitness of the formulated correlation as well as the traditional correlations are discussed.

2. Theory

Generally, mass transfer through a porous membrane in the membrane distillation (MD) process can be governed by different mechanisms: Knudsen diffusion, viscous flow, molecular diffusion or any combination thereof [6,17]. In vacuum membrane distillation (VMD), molecular diffusion is ignored when the partial pressure of air inside the membrane pores is low [4,9]. As a result, Knudsen diffusion, viscous flow or both should be considered in the VMD process [18,19]. These models propose a linear relationship between the water vapour flux (J) and the water vapour pressure difference (ΔP) across the membrane [14,20]:

$$J = C\Delta P = C(P_I - P_P) \tag{1}$$

where C is the net VMD coefficient which is dependent on the membrane geometric structure and on the temperature. P_I and P_P are the partial pressure of water vapour at the membrane surface on the feed side and that on the permeate side, respectively.

The Knudsen number (Kn), defined as the ratio between the mean free path and the pore size, is used to determine the mechanism that dominates mass transfer through a membrane.

$$Kn = \frac{\lambda}{d_p} \tag{2}$$

where λ and d_p are the mean free path and pore size, respectively. In VMD, desalination is a single- component transport process when NaCl aqueous solution is tested as the feed. Thus, only water vapour is transferred through the membrane pores. The mean free path of water vapour molecules is estimated as follows [4,9]:

$$\lambda = \frac{k_B T}{\sqrt{2}\pi \overline{P}\sigma^2} \tag{3}$$

where σ is the collision diameter of water vapour (i.e. 2.641 Å), k_B is the Boltzmann constant, $\overline{P}$ is the mean pressure within the membrane pores and T is the absolute temperature. One type of commercial flat-sheet polyvinylidene fluoride membrane (Westran S, Whatman) with a nominal pore size of 0.2 μm, is employed in this study. Under the experimental conditions applied in this work, feed temperatures ranging between 65 and 90 °C under a constant permeate pressure of 14.5 kPa, the mean free path of water vapour molecules varies between 0.38 and 0.76 μm. Thus, the value of Kn varies from 1.9 to 3.8 for a pore size of 0.2 μm. Consequently, both Knudsen diffusion and viscous flow should be considered in the VMD process [6,9]. In this case, the Kinetic Theory of Gases, or more precisely the Dusty gas model, suggests that a transition mode of the Knudsen-viscous mechanism governs water vapour transport through membrane pores [16,21]:

$$C = 1.064\frac{rs}{\tau\delta}\left(\frac{M}{RT_m}\right)^{0.5} + 0.125\frac{r^2 s}{\tau\delta}\left(\frac{MP_m}{\eta RT_m}\right) \tag{4}$$

where r is the membrane pore radius, ε is the membrane porosity, τ is the tortuosity, δ is the membrane thickness, M_w is the molecular weight of water vapour, η is the viscosity of water vapour, R is the

universal gas constant, T_m is the average temperature of the membrane, and P_m is the average partial pressure in the membrane pores. The VMD coefficient C is relied on the membrane geometric structure and on the temperature.

The geometric structure parameter $(r/\tau\delta)$ of the membrane is measured by low-range pressure gas permeation method [9,13]. N_2 gas is used as the test gas. The pressure difference across the membrane is ranging from 100 to 600 Pa. The measurement is conducted at room temperature, i.e. 25 °C. In the considered experimental conditions, the mean free path of N_2 molecules (σ of N_2 is 3.798 Å) varies between 21 and 129 μm. The corresponding Knudsen number varies between 107 and 643 in which the Kinetic Theory of Gases suggests the gas flux $\left(J_g\right)$ through the membrane is governed by the Knudsen diffusion model:

$$J_g = K_m\sqrt{M_g}\Delta P \tag{5}$$

where K_m is the permeability coefficient, M_g is the molecular weight of N_2 gas and ΔP is the pressure difference across the membrane. The permeability coefficient is further defined as follows

$$K_m = \frac{1.064}{\sqrt{RT_m}}\left(\frac{rs}{\tau\delta}\right). \tag{6}$$

Low pressure range is selected in order to preserve the original physical properties of the membranes. A small change on the membrane structure can be sensitively detected. The gas flow rate across the membrane is low so that to minimise the human error during the measurement. The membrane parameter $(\varepsilon/\tau d)$ is obtained from the slope of the plot J_g versus ΔP.

Fig. 1 shows the heat and mass transfer in the cross-flow VMD process. For non-ideal binary mixtures such as NaCl aqueous solutions, the partial pressure of the water vapour on the feed side is evaluated as follows [22,23]:

$$P_I = (1 - n_{s,I})\gamma_W P_W^\circ \tag{7}$$

where $n_{s,I}$ is the mole fraction of NaCl at the membrane surface, γ_W is the activity coefficient of water, and P_W° is the saturation pressure of pure water. The activity coefficient of water in a NaCl solution is given by [4,24]

$$\gamma_W = 1 - 0.5n_{s,I} - 10n_{s,I}^2 \tag{8}$$

The saturation pressure of pure water is estimated by the Antoine equation [8,21]:

$$P_W^\circ = \exp\left[23.1964 - \frac{3816.44}{T_I - 46.13}\right] \tag{9}$$

where T_I is the feed temperature at the membrane surface.

The partial pressure of water vapour at the membrane surface on the permeate side (P_p) is equal to the absolute pressure applied on the permeate side (P_v) [25,26]:

$$P_p = P_v. \tag{10}$$

Boundary layers are significant in the VMD process when employing a highly-permeable membrane. The solute concentration at the membrane surface may differ from that in the bulk phase. In MD, the film theory model is commonly used to describe the mass transfer of solutes through the feed boundary layer [4,27,28]:

$$J = k_L\rho\ln\left(\frac{n_{s,I} - n_{s,p}}{n_{s,b} - n_{s,p}}\right) \tag{11}$$

where k_L is the solute mass transfer coefficient in the liquid feed phase, ρ is the density of the feed solution, $n_{s,b}$ is the molar fraction of salt in the feed bulk phase and $n_{s,p}$ is the molar fraction of salt in the permeate phase. To test NaCl solutions as feed solutions, the liquid phase is evaporated at the vapour–liquid interface while the salt is retained in the liquid feed phase. The water vapour travels through the membrane pores and is condensed as distilled water in the permeate phase. As a result, the value of $n_{s,p}$ must be equal to
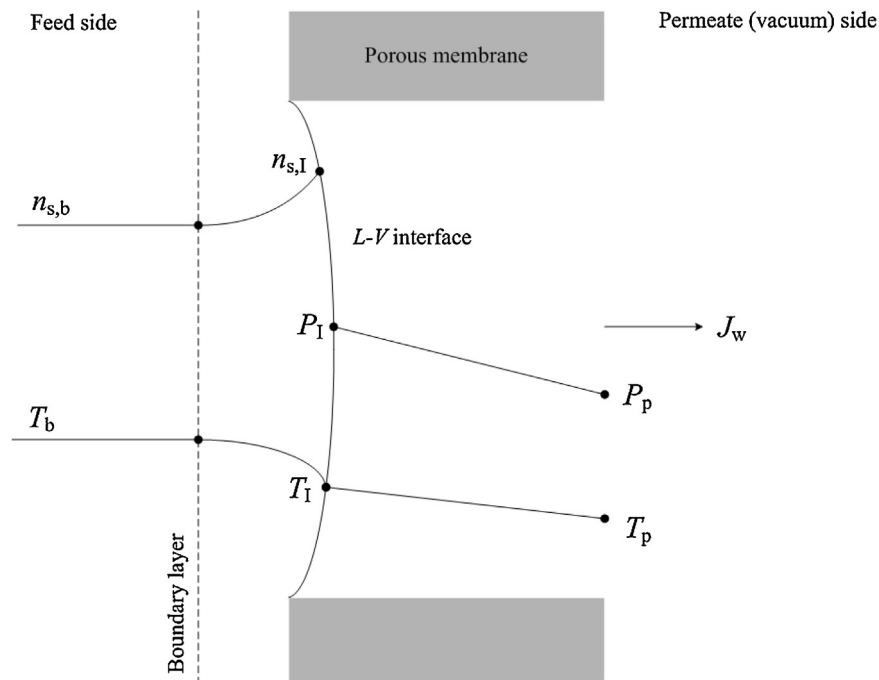
Fig. 1. Hypothetical diagram of the heat and mass transfer in the cross-flow VMD process.

zero; thus, Eq. (11) is reduced to the following expression [1,17]:

$$J = k_L \rho \ln\left(\frac{n_{s,I}}{n_{s,b}}\right) \qquad (12)$$

Because of the vacuum pressure applied on the downstream side of the membrane, the boundary layer on the permeate side is negligible [9,29].In the porous membrane used in MD, heat is transferred together with the mass flux through the membrane pores. Heat is also transferred by conduction through the membrane matrix and the vapour as well as air trapped inside the pores. The heat transfer across the membrane (Q_m) can be derived as [6]:

$$Q_m = J\Delta H_v + \frac{k_m}{\delta}(T_{I,f} - T_{I,p}) \qquad (13)$$

where ΔH_v is the latent heat of vaporisation, k_m is the thermal conductivity of the membrane, and $T_{I,f}$ and $T_{I,p}$ are the temperatures of membrane interfaces on the feed side and on the permeate side, respectively. The thermal conductivities of PVDF range from 0.17 to 0.22 W/m K. When the porosities of the porous membranes are significant (>35%), the thermal conductivities of the membranes can be reduced to between 0.04 W/m K and 0.06 W/m K [9,17]. Additionally, the thermal conductivities of the water vapour and air are respectively 0.024 and 0.032 W/m K at 100 °C. In VMD, the vacuum pressure applied on the downstream side of the membrane is able to remove the water vapour and air that trapped inside the pores. Hence, the thermal conductivity of the porous PVDF membrane is further reduced. As a result, the heat transfer by the conduction through the membrane is usually neglected in VMD process [9,21]:

$$Q_m = J\Delta H_v \qquad (14)$$

Additionally, a perforated metal support is in intimate contact with the membrane in order to prevent the membrane from rupturing. The heat transfer resistance due to this support is neglected in this study as its porosity is high i.e. approximately 74%. The vapour is directed by the vacuum suction and then condensed in the cold trap.

The boundary layer that develops next to the membrane surface can cause the temperature at the membrane surface to differ from the temperature in the bulk phase. The heat transfer coefficient in the boundary layer can affect the heat flux and the vapour flux through the membrane. The heat transfer through the boundary layer in the liquid feed phase (Q_f) is expressed as follows [15,18]:

$$Q_f = h_L(T_b - T_I) \qquad (15)$$

where h_L and T_b are the heat transfer coefficient in the liquid feed phase and the bulk feed temperature, respectively.

By neglecting the heat transfer resistance through the vacuum side, the energy balance of the process can be expressed as follows [18,29]:

$$J\Delta H_v = h_L(T_b - T_I) \qquad (16)$$

Heat and mass transport in MD can be limited by the boundary layers in the liquid feed phase, the membrane itself or both. In general, the magnitudes of the boundary layer resistances in the feed phase can be measured by the corresponding polarisation coefficients. The resistances due to the thermal and concentration boundary layers can be measured by the temperature polarisation coefficient (TPC) and concentration polarisation coefficient (CPC), respectively [9]:

$$TPC = \frac{T_I}{T_b} \qquad (17)$$

$$CPC = \frac{n_{s,b}}{n_{s,I}} \qquad (18)$$

The heat and mass transfer resistances in the feed phase affect the VMD process when the values of the TPC and CPC are less than 1. The effectiveness of the feed flow channel in accommodating heat and mass transfer is good when the values of TPC and CPC approach unity.

Vapour pressure is a function of temperature and concentration in the desalination process. Because the resistance on the permeate side is neglected in VMD, the total resistance is composed of the resistances in the feed boundary layer (R_L) and in the membrane (R_m). These resistances can be evaluated as follows [30]:

$$R_L = \frac{p_b - p_I}{J} \qquad (19)$$

$$R_m = \frac{p_I - p_p}{J} \qquad (20)$$

where p_b is the vapour pressure in the bulk phase.

Both the temperature and concentration at the membrane surface cannot be measured experimentally, but they can be estimated using Eqs. (16) and (12), respectively. The heat and mass transfer coefficients can be calculated from the corresponding

Table 1
Summary of the Nusselt and Sherwood correlations commonly used for the estimation of MD heat and mass transfer in feed flow channels under laminar flow.

No.	Heat and mass transfer correlation	Characteristics of membrane module
(1)	$Nu = 1.86(RePrd_h/L)^{1/3}$	Flat-sheet membrane module; horizontal position; $L = 55$ mm [32]
	$Sh = 1.86(ReScd_h/L)^{1/3}$	Flat-sheet membrane module; vertical and horizontal positions; $L = 100$ mm [30,33]
		Flat-sheet membrane module; horizontal position; $L = 100$ mm [34]
		Flat-sheet membrane module; horizontal position; $D = 58$ mm [21]
		Hollow-fibre membrane module; horizontal position; $L = 140$ mm [35]
(2)	$Nu = 1.62(RePrd_h/L)^{1/3}$	Flat-sheet membrane module; $L = 125$ mm [36]
	$Sh = 1.62(ReScd_h/L)^{1/3}$	
(3)	$Nu = 4.36 + \dfrac{0.036(RePrd_h/L)}{1 + 0.0011(RePrd_h/L)^{0.8}}$	Capillary and tubular membrane modules; $L = 0$–100 mm [37]
	$Sh = 4.36 + \dfrac{0.036(ReScd_h/L)}{1 + 0.0011(ReScd_h/L)^{0.8}}$	Flat-sheet membrane modules; vertical position; $L = 100$ mm [38]
(4)	$Nu = 0.74Re^{0.2}(GrPr)^{0.1}Pr^{0.2}$	Flat-sheet membrane modules; vertical and horizontal positions; $L = 300$ – 660 mm [39,40]
	$Sh = 0.74Re^{0.2}(GrSc)^{0.1}Sc^{0.2}$	

Nusselt (Nu) and Sherwood (Sh) numbers:

$$h_L = \left(\frac{k_T}{d_h}\right) Nu \qquad (21)$$

$$k_L = \left(\frac{D_s}{d_h}\right) Sh \qquad (22)$$

where k_T, D_s and d_h are the thermal conductivity of the feed solution, the solute diffusivity and the hydraulic diameter, respectively.

The Nusselt and Sherwood numbers are usually estimated based on various existing correlations developed for non-porous and rigid walls. The analogy between the Nusselt and Sherwood correlations are commonly employed in MD to determine the heat and mass transfer coefficients simultaneously [13,24,31]. Different flow regimes in the feed channel require different correlations. The Reynolds numbers explored in the present study ranged from 150 to 1400, under which the feed flow is always laminar ($Re < 2100$). The existing correlations for laminar flow are listed in Table 1. These correlations are commonly used to estimate the heat and mass transfer coefficients in most of the MD literature. These correlations are considered in this study because the lengths (L) as well as the hydraulic diameters (d_h) of the feed flow channels are relatively short, i.e. 55–660 mm. Moreover, the length of the feed flow channel of the flat-sheet membrane module used in this study falls within this range, i.e. 102 mm.

In re-evaluating the heat and mass transfer coefficients for a rectangular cross-flow channel with a porous and phase-change wall, the general forms of the heat and mass transfer correlation, respectively, can be expressed as follows [13,15]:

$$Nu = aRe^b Pr^c \qquad (23)$$

$$Sh = aRe^b Sc^c \qquad (24)$$

where Pr and Sc are Prandtl and Schmidt numbers; a, b and c represent the characteristic constants of the module design and liquid flow regime. Based on the analogy between heat and mass transfer, Eqs. (23) and (24) can be rearranged as follows:

$$NuPr^{-c} = ShSc^{-c} \qquad (25)$$

It should be noted that the semi-empirical Nusselt correlation, which was developed specifically for the same rectangular cross-flow flat-sheet membrane module in our previous study, was considered in this work, for which the values of a, b and c were 2.76×10^{-3}, 0.97 and 3.7909, respectively [16]. The schematic diagram of the rectangular cross-flow flat-sheet membrane module is shown in Fig. 2.

The physical properties of the NaCl solution employed were evaluated at the mean temperature between the inlet and outlet bulk temperatures. The equations defining physical properties such as density, viscosity, heat capacity, thermal conductivity and solute diffusivity are listed in Table 2.

In this work, the theoretical flux was calculated by using Eq. (1). Thermal and concentration layers were considered at the membrane surface on the feed side because NaCl solutions were tested as the feed solutions. First, the bulk feed temperature $T_b = (T_{fi} + T_{fo})/2$ was calculated as the mean value between the inlet and outlet module temperatures. The inlet temperature T_{fi} and outlet temperature T_{fo} of the module were recorded during the experiments. The bulk feed concentration $n_{s,b} = (n_{fi} + n_{fo})/2$ was calculated as the average value between the inlet and outlet module temperatures. The inlet concentration n_{fi} and outlet concentration n_{fo} of the module were determined by the conductivity values. The Re, Pr and Sc were calculated at the bulk feed temperature and concentration. The heat transfer coefficient h_L and the mass transfer coefficient k_L were calculated from the semi-correlations as listed in Table 1 as well as Eq. (25) with $c = 3.7909$. Next, the temperature at the membrane surface T_I was obtained from Eq. (16) and the solute concentration at the membrane surface $n_{s,I}$ was worked out from Eq. (12). The flux J in Eqs. (12) and (16) were obtained from the experiments. It should be noted that different values of T_I and $n_{s,I}$ was obtained from different correlations.

A correction factor $(\mu_b/\mu_I)^{0.14}$ was employed to calculate the new values of Nu as there was a great temperature difference between the bulk and the membrane surface ($\Delta T > 10^\circ C$). Then, a new T_I was calculated from Eq. (16). However, the concentration difference between the bulk and the membrane surface was negligible (i.e. Δn_s ranges from 0.2 to 3.7% by using the existing correlations and 10^{-6} to 10^{-5}% by using the correlation developed in [16]). The corresponding VMD coefficient C and vapour pressure at the membrane surface P_I were respectively calculated from Eqs. (4) and (7). Finally, the theoretical flux was estimated from Eq. (1).

Next, the temperature polarisation coefficient (TPC) and the concentration polarisation coefficient (CPC) were calculated from Eqs. (17) and (18), respectively by using the T_I and $n_{s,I}$ which obtained from the previous steps. The resistances in the feed

Feed outlet

PVDF membrane

~ 23 mm

Feed inlet

Bolt and nut

102 mm

13 mm

Gasket

Dimensions of the liquid flow channel
Length: 102 mm
Width: 70 mm
Height: 13 mm

Perforated metal support

To vacuum pump
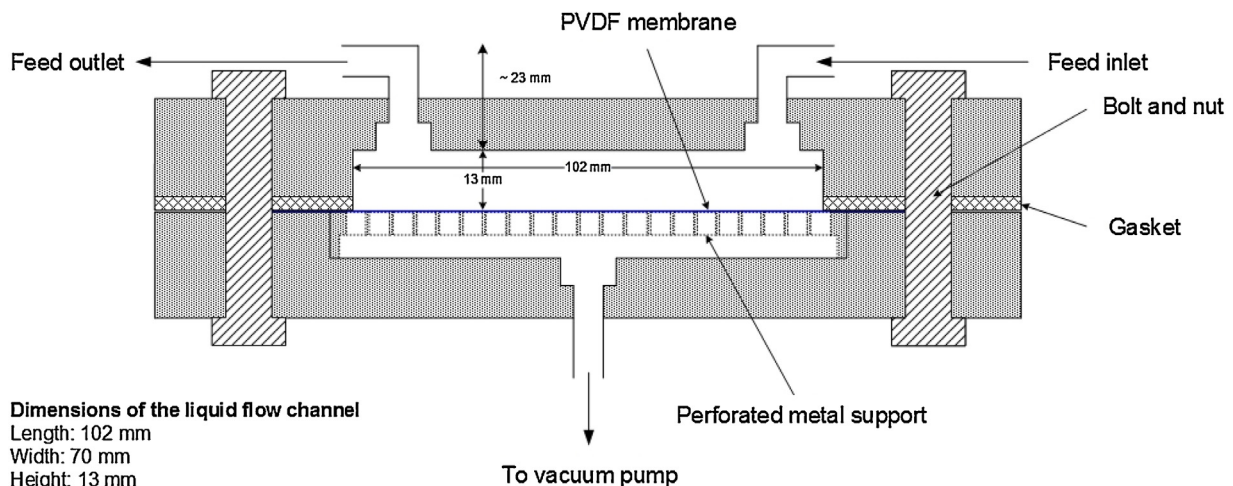
Fig. 2. Cross-sectional view of the rectangular cross-flow flat-sheet membrane module in scale 1:1.

Table 2
Equations for estimating the physical properties of the NaCl solution.

Equations	Remarks
Density: $\rho = 980 + 1950 n_{s,b}$	Temperature range from 50 to 90 °C [41]
Viscosity: $\mu =$	Can be correlated within $\pm 4\%$ [41]
$\left(8.7 \times 10^{-4} - 6.3 \times 10^{-6} T \right) \left(1 + 12.9 n_{s,b} \right)$	
Heat capacity: $C_p = 4180 - 8370 n_{s,b}$	Temperature range from 50 to 90 °C [41]
Thermal conductivity: $k_T =$	Can be correlated within $\pm 4\%$ [41]
$\left(0.608 + 7.46 \times 10^{-4} T \right) \left(1 - 0.98 n_{s,b} \right)$	
Solute diffusivity: $D_s = 8.928 \times 10^{-14} T^{\circ} \frac{(1/n_+ + 1/n_-)}{(1/\lambda_+ + 1/\lambda_-)334\mu} T.$	is is the Nernst-Haskell equation [42]. $T^{\circ} = 298.15$K; n_+ and n_- are the valences of the cation and anion, respectively at 25 °C; λ_+ and λ_- are the limiting ionic conductances in the dilute solution at 25 °C; and μ is the viscosity in centipoises unit which is evaluated at T

boundary layer and in the membrane were worked out from Eqs. (19) and (20), respectively.

3. Experimental

3.1. Gas permeation test

The low-range pressure gas permeation test used in this work is presented in Fig. 3. Pure N_2 was used as the test gas. The experiment was carried out at a room temperature of 25 °C. The flat-sheet Westran S PVDF membrane was placed inside the rectangular membrane module. The membrane module comprised of a gas inlet and a gas outlet. The gas pressure was controlled by using a needle valve. The upstream pressure was varied in a low-range pressure of 100–500 Pa, whereas, the downstream pressure was kept constant at atmospheric pressure. The pressure difference between the upstream and downstream sides of the membrane was measured by using a digital manometer (TPI 625, Korea). The membrane samples were in dry condition.

Approximately 10–15 mL of soap solution was poured into an acrylic pipe. After a desired pressure difference was set on the digital manometer using the needle valve, the acrylic pipe was shaken slowly and carefully to obtain a soap film. The gas velocities were determined by measuring the time taken by the soap film to rise 20 cm in the acrylic pipe (cross- sectional area $\approx 20 \, \text{cm}^2$) open to the atmosphere.

3.2. Cross-flow vacuum membrane distillation (VMD) experiment

Analytical- grade sodium chloride, NaCl ($\geq 99\%$) purchased from Qrëc, USA, was dissolved in distilled water to prepare feed solutions. The cross-flow vacuum membrane distillation (VMD) experimental setup employed in this study is shown in Fig. 4. The feed solution was pumped using a calibrated digital gear pump (Micropump Drives 75211-35 & Pump head 07003-04, Cole-Parmer Instrument Co., Illinois, USA) through a heating bath (Model 9012A12E, Polyscience, Niles, IL USA), and then it entered the membrane module. The cross-sectional view of the membrane
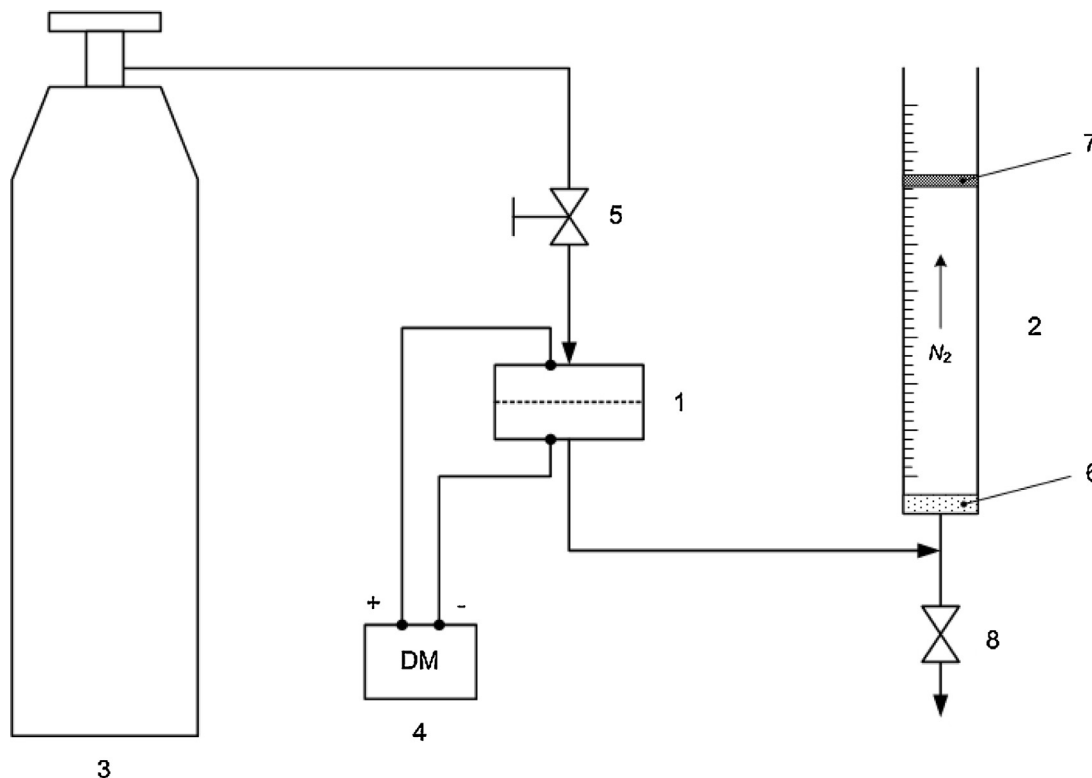
Fig. 3. Low-pressure gas permeation test for membrane permeability measurement (not to scale). 1: Module with a flat membrane; 2: acrylic pipe; 3: N_2 gas reservoir; 4: digital manometer; 5: needle valve; 6: soap solution; 7: a thin soap film; 8: ball (drain) valve.
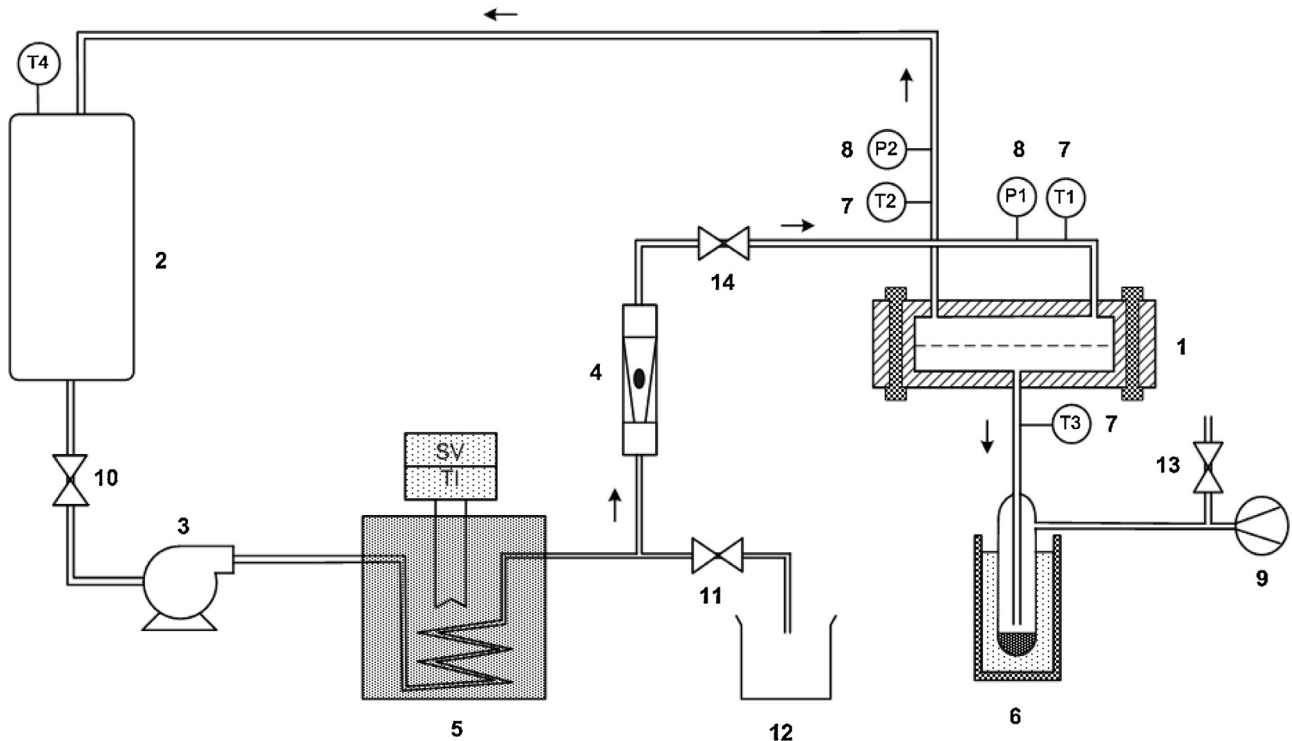
Fig. 4. Schematic diagram of physical flow of the experimental VMD apparatus. 1: membrane module with a flat membrane as shown in Fig. 2; 2. Feed reservoir; 3. Feed pump; 4: rotameter; 5: temperature control bath with heating coil; 6: cold trap housed in dewar; 7: temperature transmitters; 8: pressure gauges; 9: vacuum pump; 10: feed valve; 11: rejection discharging valve; 12: beaker for rejection collection; 13: vent valve; 14: standby valve.

module is shown in Fig. 2. The effective membrane area was 71.40 cm^2. Two digital temperature transmitters (T16LT2, Cecomp Electronics, Inc., Libertyville, IL, USA) were installed on the feed inlet and outlet, and one unit on the module downstream side, each to one significant figure. The temperature transmitters were calibrated and the calibrated values were compared with the calibrated temperature value of the heating bath. A vacuum on the

downstream side was created by a vacuum pump (Rocker 300, Today's Instruments Co., Ltd., Taiwan) which was equipped with a vacuum gauge pressure. A cold trap, refrigerated by liquid nitrogen, was used to condense the water vapour.

The concentrations of NaCl in the feed solutions and the permeates were measured by using a conductivity meter (CON
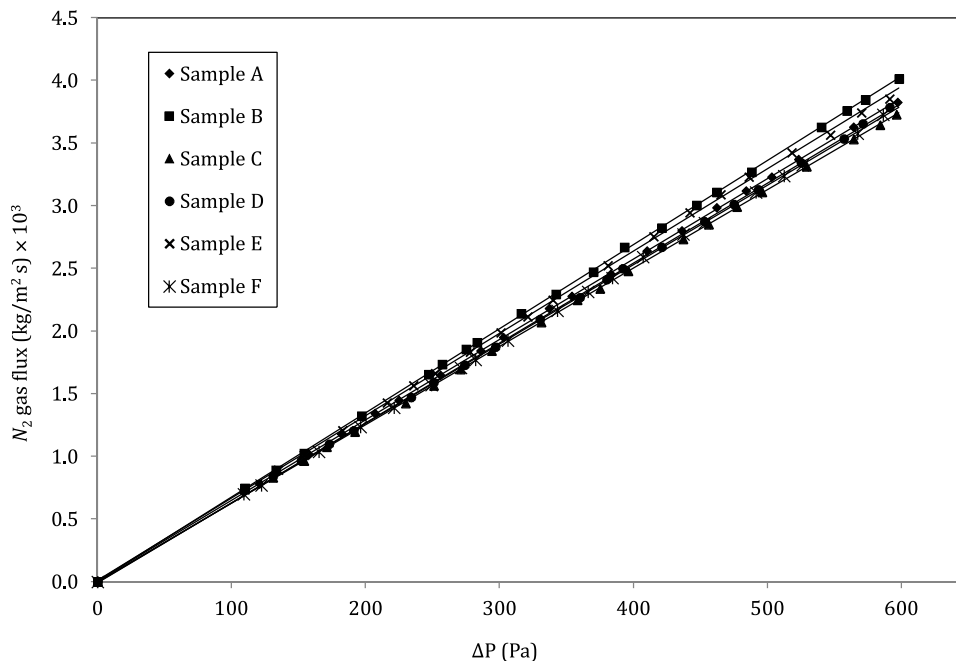
Fig. 5. The measurement of membrane permeability reported as N$_2$ gas flux versus the gas pressure difference for six samples of the Westran S membrane. The solid lines are the Knudsen diffusion fits of the data.

1500, Eutech Instrument Pte Ltd., Ayer Rajah Crescent, Singapore). The conductivity meter was calibrated before used.

The experimental flux was determined by the following equation:

$$J = \frac{m}{A \times \Delta t} \tag{26}$$

where m is the total mass of water vapour that permeates through the membrane, A is the effective membrane area, and Δt is the operation time. Each experiment was repeated at least two times in order to evaluate the reproducibility of the results. At the end of each experiment, the weight loss of the liquid feed was compared with the weight gain of the condensed permeate. A good agreement was found, that was below 5%.

4. Results and discussion

4.1. Membrane permeability

Graphs of J_g versus ΔP were plotted in order to obtain the permeability coefficient (K_m) for the Westrans S membranes as shown in Fig. 5. The average measured value of the K_m for the Westran S membranes used in this work is $(3.16 \pm 0.08) \times 10^{-5}$ mol$^{1/2}$ s m^{-1} kg$^{-1/2}$, which is of the same order of magnitude as the value of the commercial membranes employed in the literature [27,43]. The nominal pore size of the Westran S membrane is 0.2 μm (provided by the manufacturer). The membrane parameter ($\varepsilon/\tau\delta$) of the membrane was calculated based on Eq. (6). The values of the membrane parameter ($\varepsilon/\tau\delta$) were ranging from 14000 to 17000 m^{-1}

4.2. Performance of desalination by VMD

The effect of process conditions on the VMD flux was investigated. The parameters varied in this work were the feed flow rate (Q_f), feed temperature (T_f) and feed concentration of NaCl (C_f). Two groups of experiments were carried out. In the first group, the fluxes were measured by changing the feed temperature from 65 to 90 °C for each of the following feed flow rates: 300, 600, 900, 1200, 1500 and 1800 mL/min at a constant feed concentration of 2.0 wt% NaCl. In the second group, the feed concentration was varied between 0.5 and 4.0 wt% NaCl for each of the feed flow rates 300, 600, 900, 1200, 1500 and 1800 mL/min at a constant feed temperature of 80 °C.

It is worth noting that the temperatures at the module inlet strongly deviated from the temperatures set at the heating circulator, i.e. the temperature deviations varied between 11.1 and 21.8 °C. Under these conditions, the Reynolds numbers range from 150 to 1400, the Prandtl numbers range from 2.8 to 3.9 and the Schmidt numbers range from 120 to 240. In all of the experiments, the pressure on the vacuum side was maintained at a value of 14.5 kPa.

The relationships between the feed flow rates and the fluxes at different feed temperatures and a constant feed concentration of 2.0 wt% NaCl are presented in Fig. 6. As shown, the flux increases with the feed flow rate. The dependence of the flux on the feed flow rate indicates the presence of boundary layers in the liquid feed phase. At a high feed flow rate, the heat and mass transport from the bulk feed to the membrane surface are enhanced, and the temperature and the concentration at the membrane surface approach the corresponding temperature and concentration in the bulk phase, resulting in a greater flux. Overall, the fluxes are greater than 5 kg/m^2 h. The Westran S membrane is a highly permeable membrane that is suitable for desalination applications using VMD. As a result, the effect of polarisation boundary layers on the fluxes should not be ignored in this work [9].

Fig. 7 depicts the experimental flux as a function of the feed temperature for different feed flow rates. The results show that the flux increases with the both flow rate and temperature of the feed solution. The flux increases exponentially with the feed temperature. These trends can be attributed to the exponential increase in the water vapour pressure with temperature as indicated by the Antoine equation. The experimental data were fitted to Arrhenius-type correlations represented by the solid lines, i.e. $J \propto \exp(-\Delta H_v / RT_f)$, with correlation coefficients greater than 0.96. The results suggest that the experimental method is suitable and sufficient.

The effect of the feed flow rates on the fluxes at different feed concentrations is shown in Fig. 8. At a constant feed temperature of 80 °C, the flux increases with the feed flow rate. The dependence of the flux on the feed flow rate denotes the existence of polarisation layers in the feed phase. Interestingly, the variation of the feed
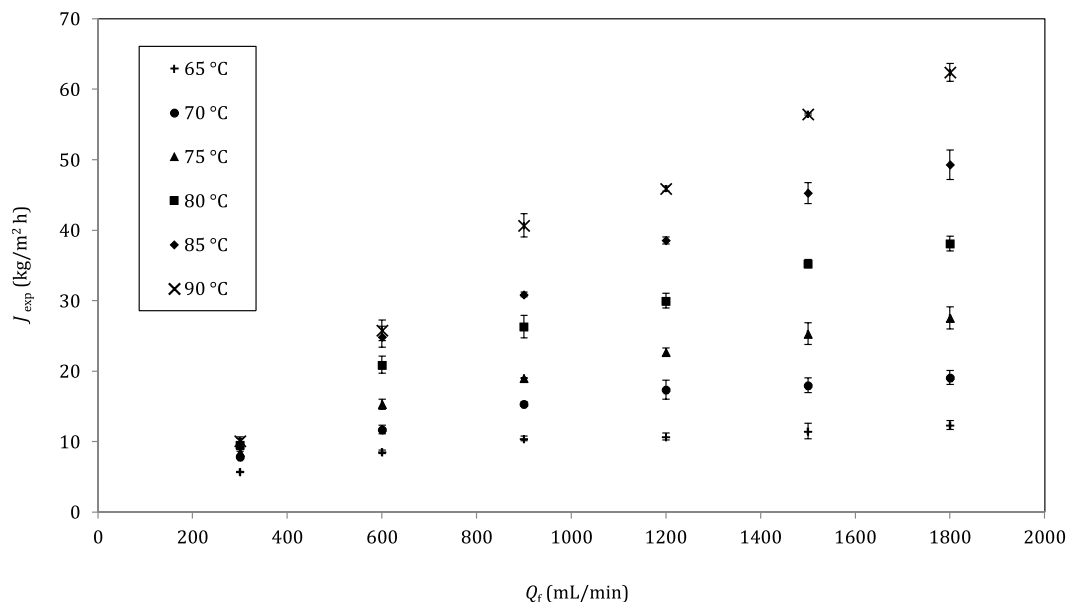
Fig. 6. Experimental flux (J_{exp}) as a function of the feed flow rate (Q_f) at different feed temperatures using 2.0 wt% NaCl solution as the feed solution.
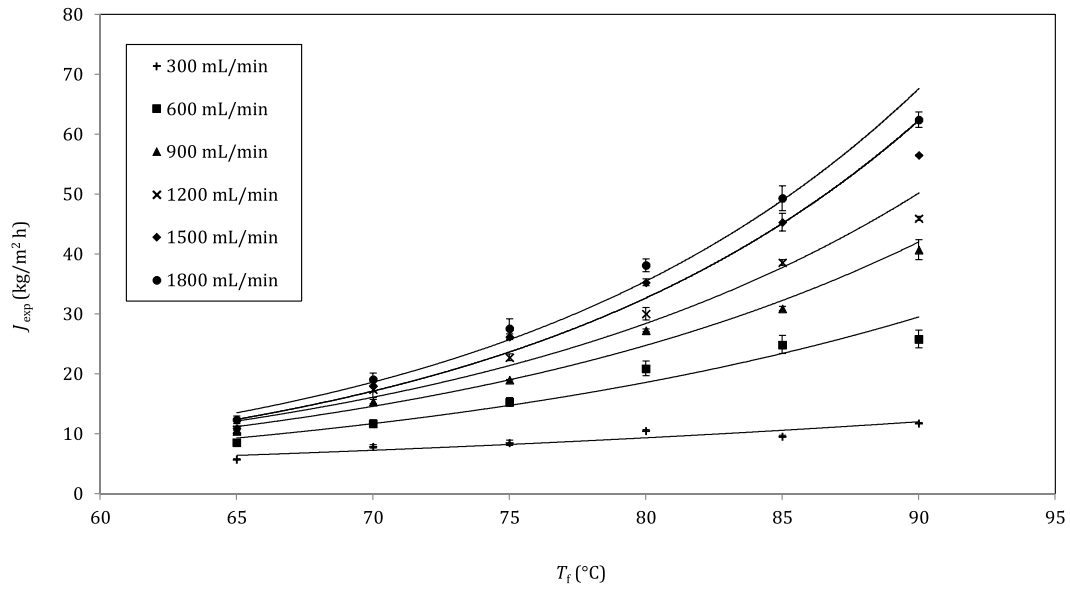
Fig. 7. Experimental flux (J_{exp}) as a function of the feed temperature (T_f) at different feed flow rates using 2.0 wt% NaCl solution as the feed solution. The solid lines are the Arrhenius fits of the data.

concentration from 0.5 to 4.0 wt% NaCl does not affect the flux significantly, as shown in Fig. 9. These experimental results are in agreement with Eq. (7) which indicating that the NaCl concentrations between 0.5 and 4.0 wt% have almost no effect on the partial pressure of the water vapour essentially, because the activity coefficient of water in the NaCl solutions is close to 1.

The measured conductivity values of the permeates were between 1.1 and 1.5 μS/cm, whereas the measured conductivity values of the feed solutions ranged from 9400 to 64800 μS/cm at room temperatures of 23–27 °C. The rejections of NaCl were 100%, which suggested no solute permeation.

The error bars corresponding to each point reported in Figs. 6–9 were less than 6%. The percentages of the deviations were small and the experimental data were acceptable for the ensuing evaluations.

4.3. Validation of correlations

The purpose of this section is to verify the applicability of various Nusselt and Sherwood correlations for desalination via the VMD process. The traditional correlations listed in Table 1 as well as the correlation developed by Chiam and Sarbatly [16] were examined. The heat transfer coefficients (h_L) and the solute mass transfer coefficients (k_L) in the liquid feed phase were estimated simultaneously from the respective Nusselt and Sherwood correlations to calculate the theoretical fluxes, where the calculation procedures were described in Theory section.

Fig. 10(a) and (b) respectively report the values of Nusselt and Sherwood numbers calculated from all the correlations. The Nusselt number ranges from 7 to 30 and Sherwood number from 28 to 240 when estimated by using the traditional correlations (1)–(4). These numbers were employed to predict the theoretical fluxes
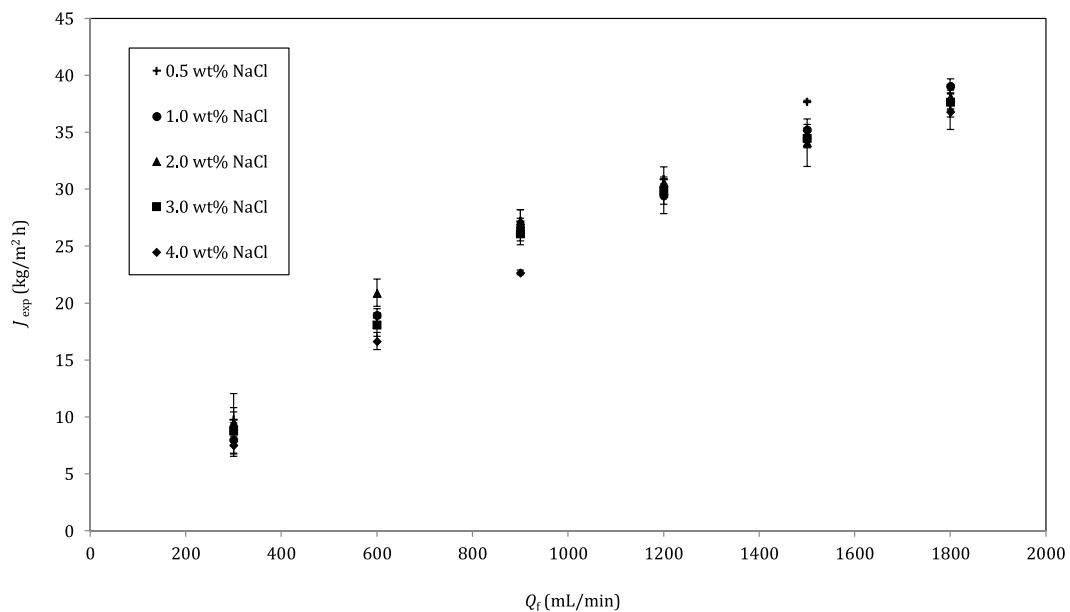
Fig. 8. Experimental flux (J_{exp}) as a function of the feed flow rate (Q_f) at different feed concentrations and a constant feed temperature of 80 °C.
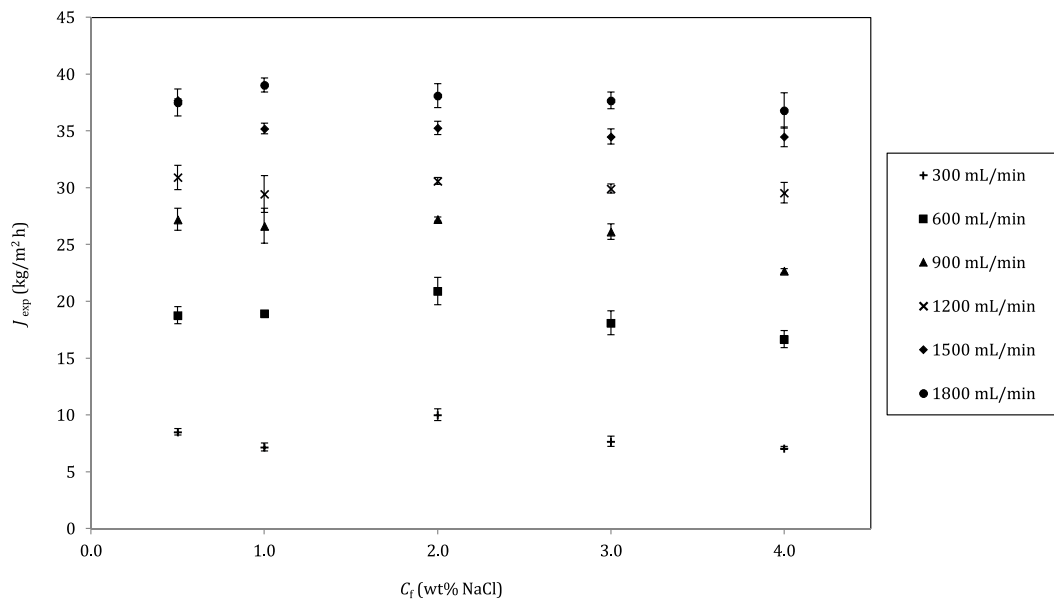
Fig. 9. Experimental flux (J_{exp}) as a function of the feed concentration (C_f) at different feed flow rates and a constant feed temperature of 80 °C.

at various process conditions of VMD. Fig. 11 shows the comparison between the calculated fluxes (J_{cal}) and the experimental fluxes (J_{exp}) for the different correlations. The results show that the fluxes predicted from the traditional correlations are less than zero. This is due to the predicted values of the partial pressure of water at the membrane surface are lower than the permeate pressure. Consequently, employing the traditional correlations for the laminar flow conditions considered ($150 < Re < 1400$) and the membrane module design used in this work can introduce a noticeable error in estimating the heat and mass transfer coefficients.

It is noted that the Nusselt correlation formulated by Chiam and Sarbatly [16] and the corresponding Sherwood correlation derived from the heat-mass transfer analogy, i.e. Eqs. (23)–(25), are acceptable for analysing the heat and mass transfer performance of VMD desalination. However, the correlations have overestimated 63% of the experimental data by deviations of more than 25%. These large deviations could be due to the thermal properties of the feed solutions. The tested correlations are developed by using distilled water as the feed solution as described in our previous paper [16]. The physical properties of water i.e. density, viscosity, heat capacity and thermal conductivity are highly dependent on temperature. In a contrary, the physical properties such as density and heat capacity of NaCl solutions are almost constant when the concentration of NaCl varies from 0.5 to 4.0 wt%. Although the water vapour flux increases with the feed temperature when distilled water as well as NaCl solutions are tested as the feed solutions, the heat transfer parameters (i.e. Re, Pr, Nu, h_L) behave differently. The deviation values of the physical properties between the distilled water and the NaCl solutions become larger especially when the mean bulk feed temperature increases.

Interestingly, the correlations developed in our previous paper [16] do fit well with the experimental data indicating relatively low fluxes. In view of the significant temperature fluctuation, the magnitudes of the deviations of the fluxes between the predicted values and the experimental values below 20% are considered agree well with the correlations. As a result, approximately 30% of the experimental fluxes do fit well with the correlations, as shown in Fig. 12. Approximately 85% of these experimental fluxes are below 25 kg/m² h, and the remaining fluxes are between 25 and 30 kg/m² h. Consequently, the relatively low feed flow rates and/or

feed temperatures, which yield fluxes below 30 kg/m² h, are investigated in the succeeding sections.

4.4. Equations of heat and mass transfer coefficients

Both the Nusselt and Sherwood correlations in Eqs. (23)–(25), with a, b and c values of 2.76×10^{-3}, 0.97 and 3.7909 [16], respectively, are further investigated. As discussed in section 4.3, the correlations are specifically valid for fluxes below 30 kg/m² h. Therefore, the feed flow rates and feed temperatures were chosen based on the corresponding experimental fluxes reported in Figs. 6–9. In the first group of experimental conditions, the selected feed temperature included the range 65 to 80 °C for each of the following feed flow rates at a constant feed concentration of 2.0 wt% NaCl: 300, 600, 900, 1200, 1500 and 1800 mL/min. In the second group of experiments, the selected feed concentrations ranged between 0.5 and 4.0 wt% NaCl for each of the feed flow rates at a constant feed temperature of 80 °C: 300, 600, 900 and 1200 mL/min.

By considering the process conditions at the corresponding experimental flux below 30 kg/m² h, the Nusselt correlation was simplified to equations that can relate the boundary layer heat transfer coefficient (h_L) and the bulk feed temperature (T_b). Similar equations were also obtained from the Sherwood correlation, which relates the solute mass transfer coefficient (k_L) and the bulk feed temperature (T_b). These equations were employed in the following simulation studies.

The effect of the bulk temperatures on the heat and mass transfer coefficients at different feed flow rates ranging from 300 to 1800 mL/min at a constant feed concentration of 2 wt% NaCl, respectively, shown in Fig. 13(a) and (b). The corresponding effect on the heat and mass transfer coefficients at different feed concentrations ranging from 0.5 to 4.0 wt% NaCl at the randomly selected feed flow rate of 600 mL/min are presented in Fig. 13(c) and (d). The solid lines were generated by least-squares analysis. Both the heat and mass transfer coefficients are suggested to be quadratic functions of the bulk feed temperatures at the corresponding correlation coefficients of $R^2 = 1.000$.

As shown in Fig. 13, the heat and mass transfer coefficients decrease as the bulk feed temperature increases. At a high feed temperature, a larger amount of heat is supplied to the membrane
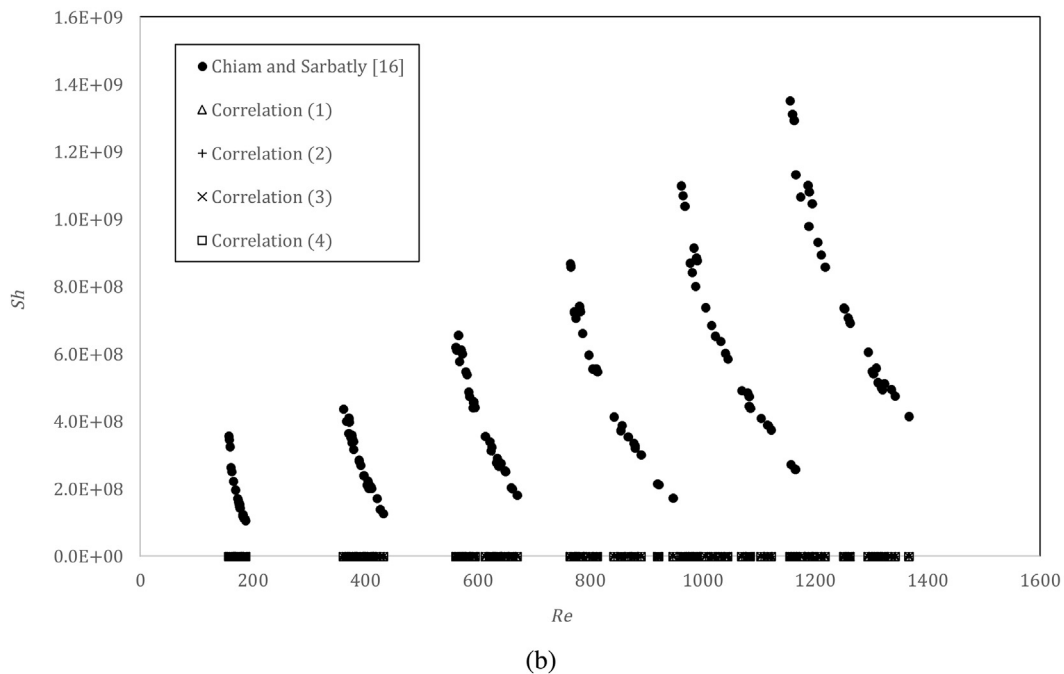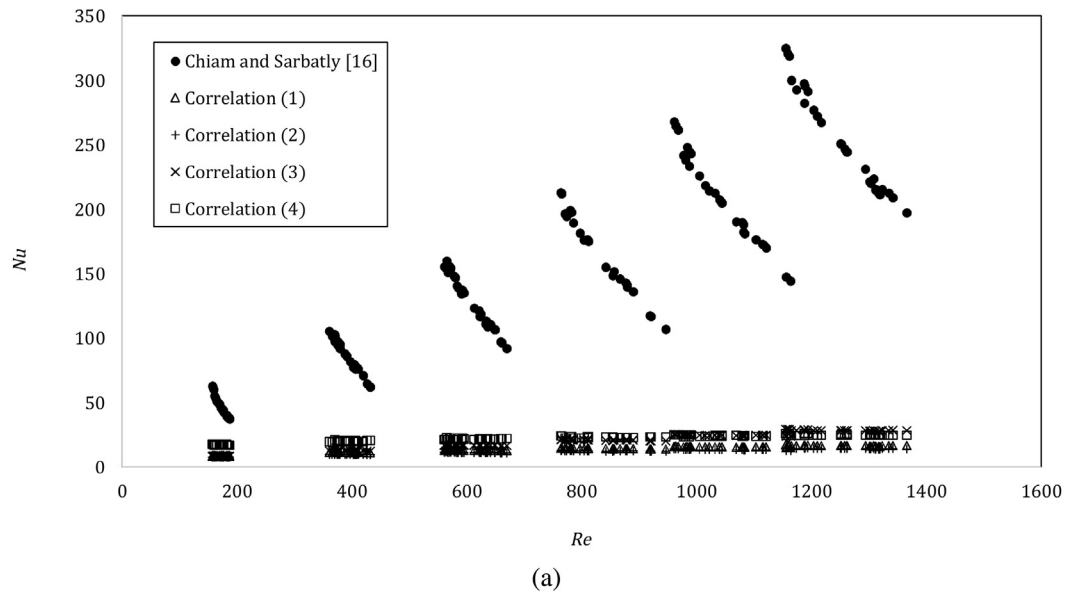
Fig. 10. (a) The Nusselt numbers calculated by using the correlations based on the experimental conditions. (b) The Sherwood numbers calculated by using the correlations based on the experimental conditions.

surface to vaporise the water; consequently, the temperature of the liquid water drops significantly at the membrane surface due to the vaporisation and the vapour transport to the cooling permeate side. The concentration of solute increases slightly when the liquid fraction reduces. The heat and mass transfer coefficients increase as the feed flow rate increases. During the experiments, the mean bulk feed temperature increases with the feed flow rate. However, the enhancement of the bulk feed temperature is small i.e. 0.5–2 °C which has no significant reduction effect on the heat and mass transfer coefficients. The effect of feed flow rate has compensated the effect of mean bulk feed temperature on the heat and mass transfer. At the high feed flow rate, the temperature and the concentration at the membrane surface approach the corresponding temperature and concentration in the bulk phase; thus, the polarisation effects decrease as the feed flow rate increases.

The graphs in Fig. 13(c) and (d) show how the heat and mass transfer coefficients increase with increasing feed concentration. Compared to the Reynolds number, the Prandtl and Schmidt numbers appear to be more influential in determining the Nusselt and Sherwood number, respectively. Unlike the empirical constants employed in the traditional correlations, where $b \cong c$, as presented in Table 1, Fig. 13(c) and (d) were generating using a c value that is approximately four times greater than the b value. It can be observed that the ratios of (μ/k_T) and (μ/D_s) increase with the NaCl concentration in the feed solution. As a result, the viscosity of the NaCl solution is recognised as a significant property affecting both the Prandtl and Schmidt numbers and also the corresponding simulated heat and mass transfer coefficients. Additionally, the physical properties of the NaCl solutions, such as density and heat capacity, are assumed to be independent of
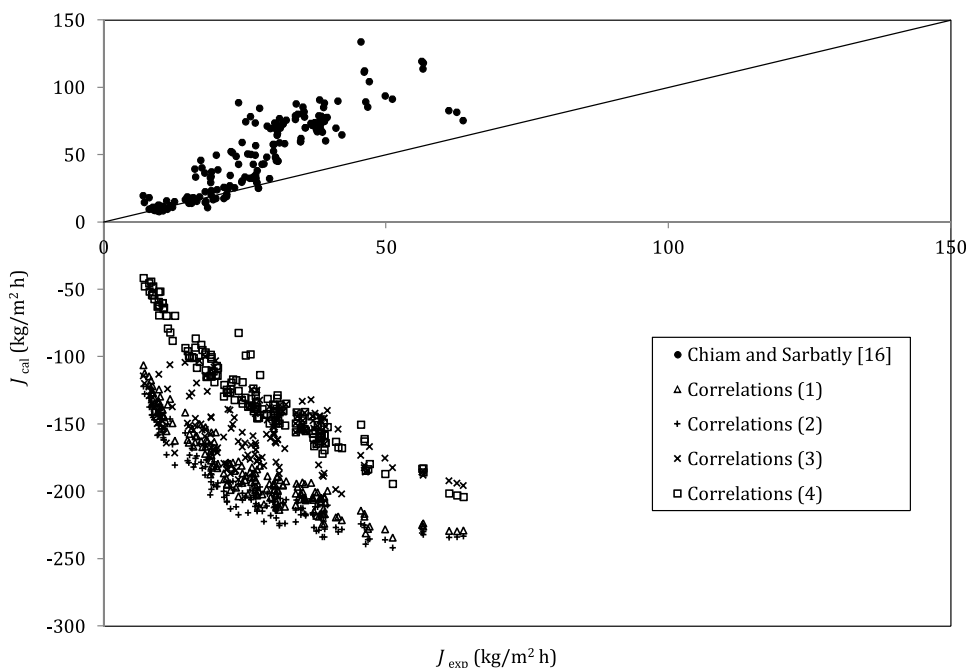
Fig. 11. A comparison of the experimental fluxes and the fluxes calculated by the correlations.

temperature (see Table 2). This explanation is adequate because the correlations were previously developed by using distilled water as the feed solution, whose physical properties are highly dependent on temperature [16].

Nevertheless, the experimental fluxes reported in Figs. 8 or 9 show almost no change with the feed concentrations ranging from 0.5 to 4.0 wt% NaCl. However, there is a discrepancy in the simulated data plotted in Fig. 13(c) and (d). It is deduced that the viscosity effect may not be the main factor that controls the flux when a NaCl solution is used as the feed solution; rather, the vapour pressure may be the most significant parameter that

determines the flux. As revealed by Schofield et al [41] in a comparative study of pure water and a 30 wt% NaCl solution tested at 81 °C in a DCMD system, a 29% reduction in vapour pressure reduced the flux by 32%, whereas the flux was reduced by 11% due to viscosity effects. In fact, the vapour pressure has no effect on heat and mass transfer parameters such as Re, Pr, Sc, Nu, Sh, h_L and k_L; instead, these parameters are dependent on the physical properties of the feed solution. In this work, the activity coefficients of water were always greater than 0.992; therefore, the vapour pressures as well as the fluxes did not change appreciably as the feed concentration were varied between
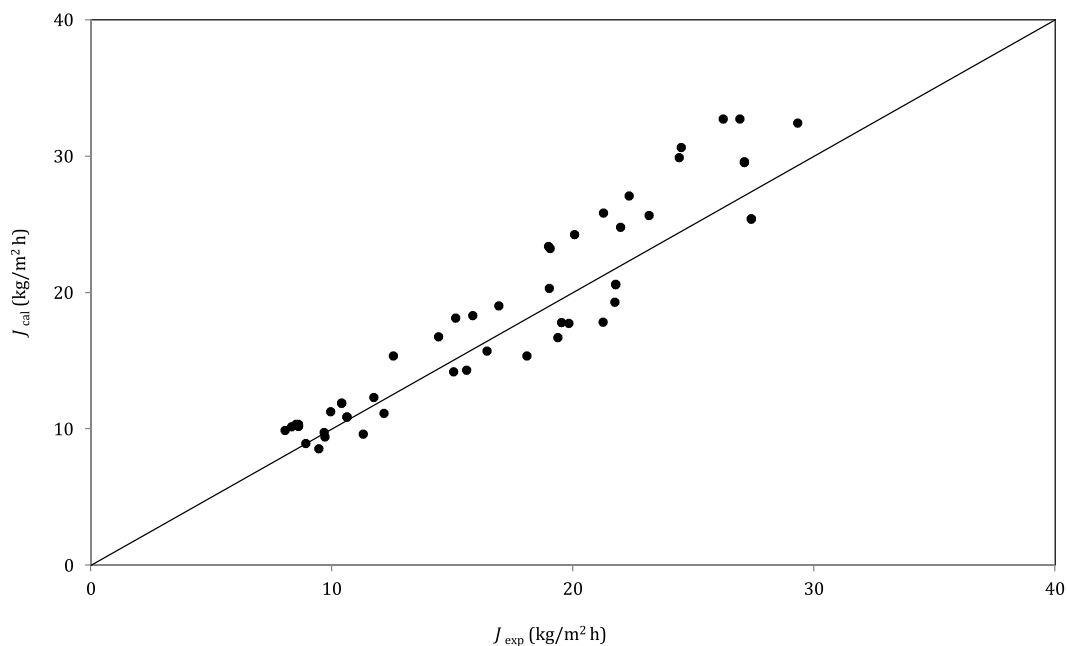
Fig. 12. The good agreement between 30% of the experimental fluxes ($<$ 30 kg/m^2 h) and the fluxes calculated by the correlations derived by Chiam and Sarbatly [16].
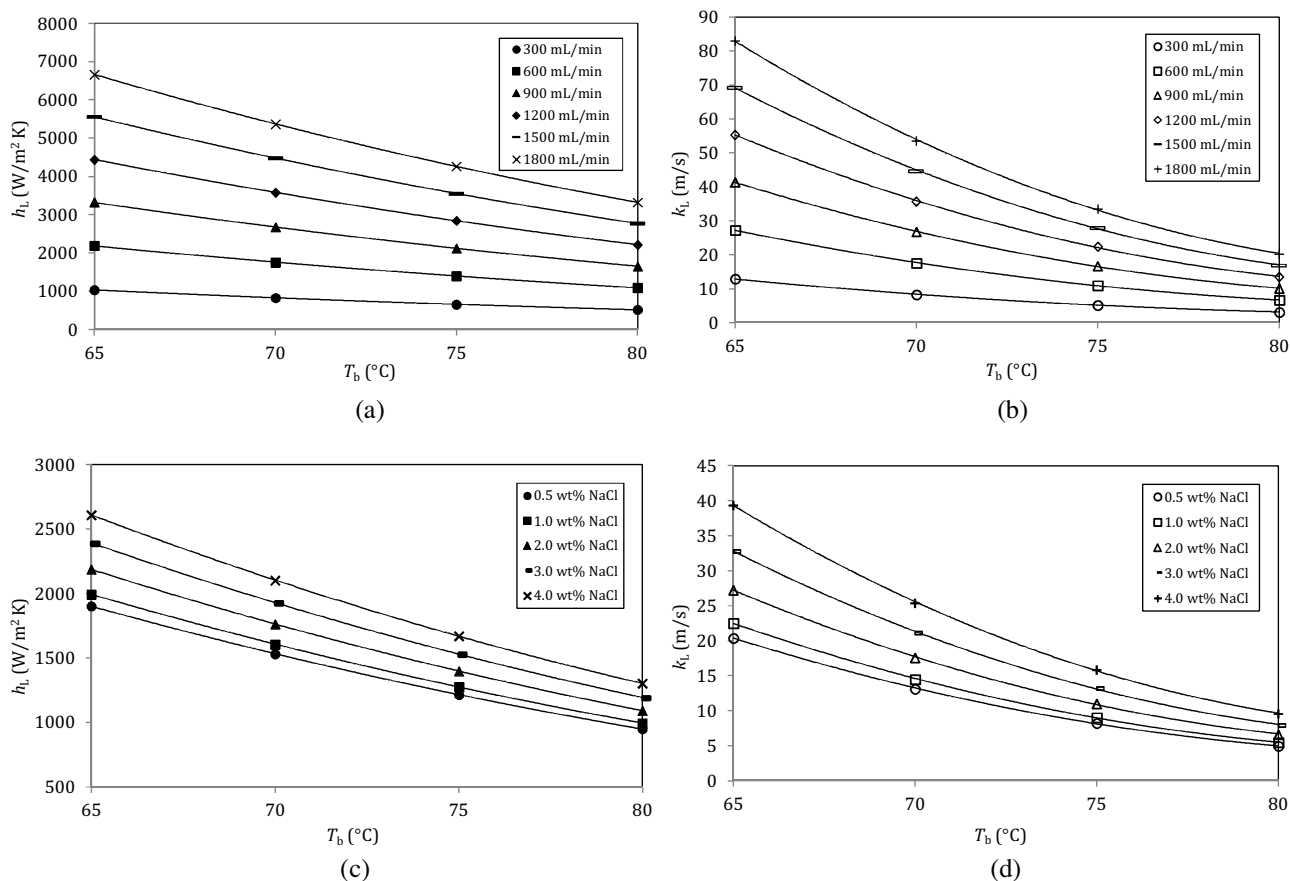
Fig. 13. Relationship between transport coefficients and feed bulk temperature (65–80 °C) for feed flow rates ranging from 300 to 1800 mL/min and feed concentrations ranging from 0.5 to 4.0 wt% NaCl.

0.5 and 4.0 wt% NaCl. Compared to the effect of the heat and mass transfer coefficients due to the ratios of (μ/k_T) and (μ/D_s), the vapour pressure on the feed side has more influential effect on the flux.

For comparison, the values of the heat and mass transfer coefficient documented in the VMD literature range from 50 to 16000 W/m^2 K [15,25,31,44] and from 10^{-4} to 10^{-6} m/s [31,45,46]. respectively. The rectangular cross-flow flat-sheet membrane module used in this work could achieve the experimental heat transfer coefficients between 1121 and 9456 W/m^2 K which fall within the reported range. Interestingly, the experimental solute mass transfer coefficients ranged from $10°$ to 10^1 m/s, which are extremely large values i.e. approaching infinity. By using the calculation procedure described in Theory section, the concentration differences between the bulk and the membrane surface are approximately 10^{-6} to 10^{-5}%. This indicates that the mass transfer resistance due to the NaCl solute in the feed phase might be negligible. As a result, the desalination process is mainly affected by the heat transfer resistance from the feed phase [9].

4.5. Polarisation effects

Based on the values of the temperature and concentration at the membrane surface, the corresponding temperature polarisation coefficient (TPC) and concentration polarisation coefficient (CPC) were obtained from Eqs. (17) and (18); the results are presented in Fig. 14. The effect of the feed temperature, feed flow rate and feed concentration on the TPC and CPC was investigated.

Fig. 14 (a) shows that the TPC decreased with increasing temperature. The temperature polarisation coefficients ranged

from 0.994 to 0.998 at a low feed temperature of 65 °C and decreased to 0.984–0.990 at a high feed temperature of 80 °C. At high temperatures, the flux was much higher than that at low temperatures, as demonstrated in Figs. 6–9. Consequently, a larger amount of heat was required to vaporise the water at the membrane surface, which caused the large difference in temperature between the bulk feed phase and the membrane surface.

Both Fig. 14(a) and (b) shows the values of the TPC at various feed flow rates. The increase in the heat transfer coefficient in the boundary layer was induced by the feed flow rate. The temperature polarisation coefficients were 0.984–0.994 at a low feed flow rate of 300 mL/min and increased to 0.990–0.998 at a high feed flow rate of 1800 mL/min. The high feed flow rate reduced the temperature difference between the bulk feed phase and the membrane surface.

The values of the TPC did not change significantly as the feed concentration varied between 0.5 and 4.0 wt% NaCl, as shown in Fig. 14(b). The temperature polarisation coefficients were 0.985–0.986 at a low feed concentration of 0.5 wt% NaCl and 0.984–0.990 at a high feed concentration of 4.0 wt% NaCl. At a constant feed temperature of 80 °C, the mole fraction and the activity coefficient of water at the membrane surface were greater than 98.5% and 0.992, respectively. These conditions contributed to the invariant partial pressure of water at the membrane surface.

Fig. 14(a) and (b) also depicts the values of the CPC. The results show that the concentration polarisation coefficients approached unity for all conditions tested. The explanation is as follows. As described in our previous paper [16], the module design employed in this work does not allow for smooth transitions of the feed
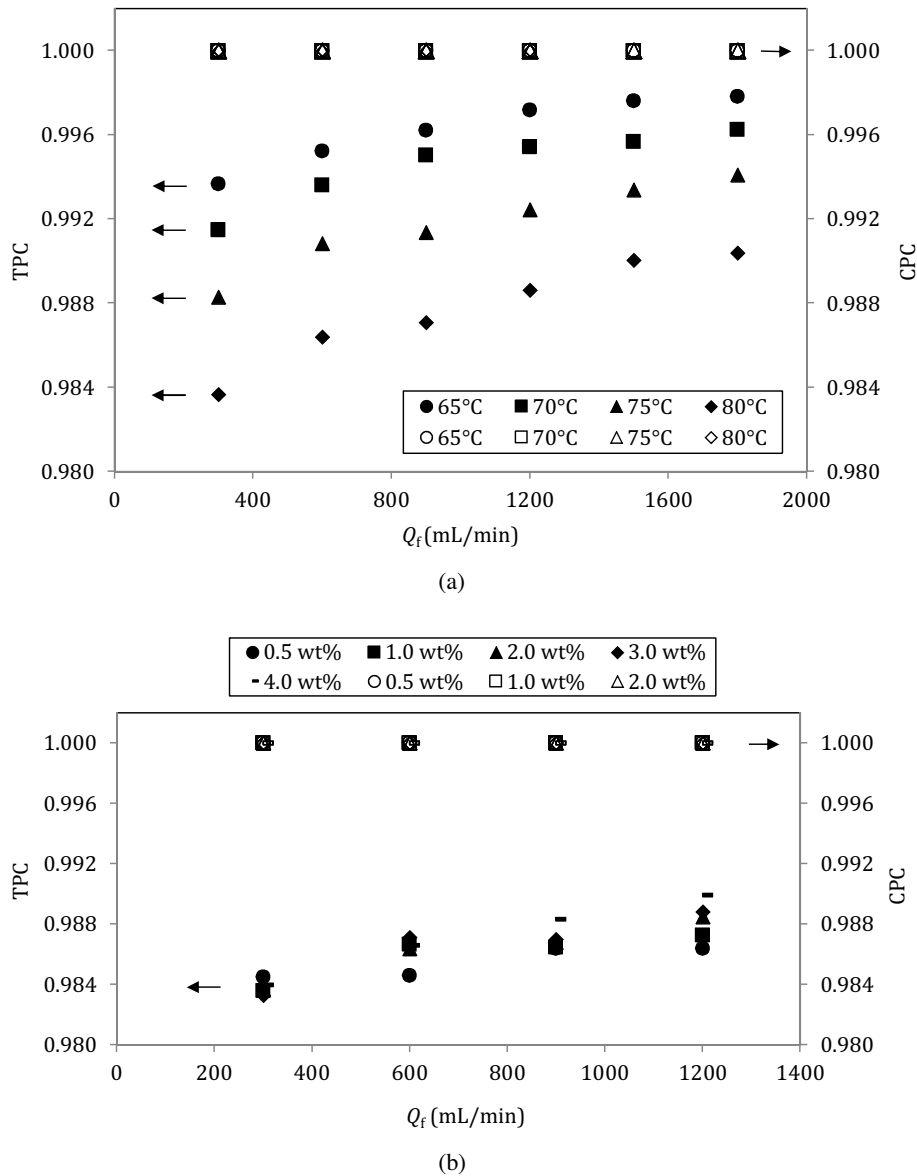
Fig. 14. Temperature and concentration polarisation coefficients for feed flow rates ranging from 300 to 1800 mL/min, feed temperatures ranging from 65 to 80 °C and feed concentrations ranging from 0.5 to 4.0 wt% NaCl.

solution at the module entrance and exit. The feed solution flowed out from the exit of the module only when the flow channel was full. As the liquid viewed like horizontal layers, the disturbance due to the bulk feed cross-flowing effect on the layers that are nearer to the membrane surface might be lesser than that on the upper layers which are nearer to the entrance and exit of the module. Furthermore, the disturbance due to the cross-flow stream will become lower if the flow channel height becomes deeper. As a result, the feed liquid layer with the initial concentration of NaCl (i.e. same with the concentration in feed bulk phase; $n_{s,I} = n_{s,b}$) that was laid next to the membrane might not be affected practically. Therefore, the values of the solute mass transfer coefficients plotted in Fig. 13 are accepted, and they approached the infinite.

The CPC values confirmed that the mass transfer in the desalination was limited by the membrane itself, i.e. governed by the Knudsen-viscous resistance. The effect of both feed boundary layer resistance and membrane resistance on the heat transfer in the desalination process is further discussed in the next sections.

4.6. Transport resistances

The effect of the considered process conditions on the transport resistances in the feed boundary layer and the membrane was further investigated. Based on the polarisation coefficients obtained, as discussed in section 4.5, the heat transfer resistance in the feed phase should not be neglected compared to the mass transfer resistance because CPC → 1. On the other hand, the membrane resistance is known to have been the main factor that controlled the mass transfer in the desalination process. The resistances in the feed boundary layer and the membrane at various process conditions were calculated as shown in Fig. 15.

The feed boundary layer resistance decreased greatly from 400–450 to 160–240 Pa m² h/kg at corresponding feed flow rates ranging from 300 to 600 mL/min, and the resistance was reduced in advance to 52–80 Pa m² h/kg at 1800 mL/min. Additionally, the feed boundary layer resistance decreased significantly from 82–211 Pa m² h/kg at a feed temperature of 80 °C to 52–162 Pa m² h/kg at 70 °C. The results demonstrate that the transport resistance in the feed boundary layer played an important role at a low feed flow
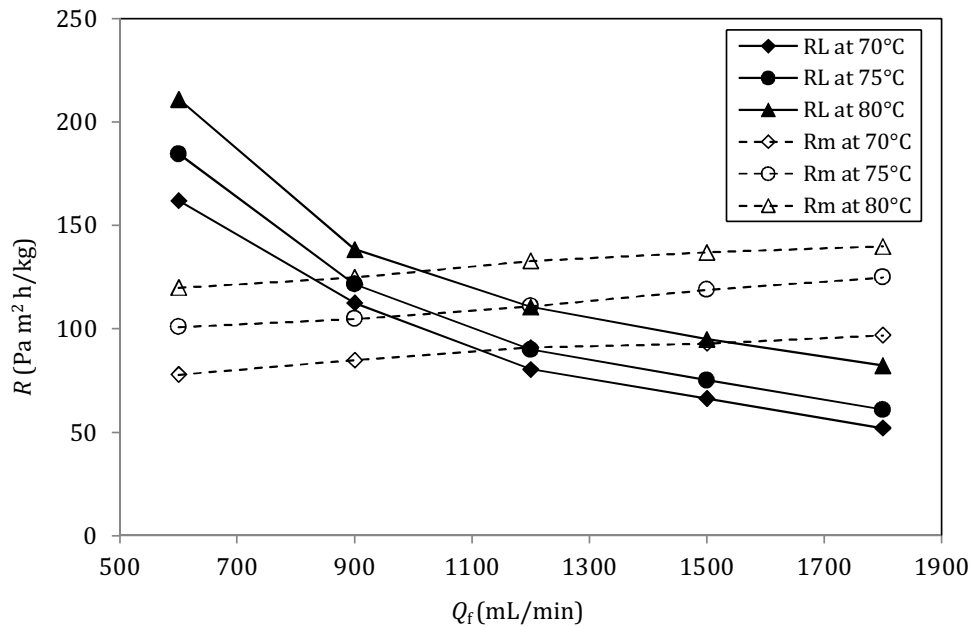
(a)
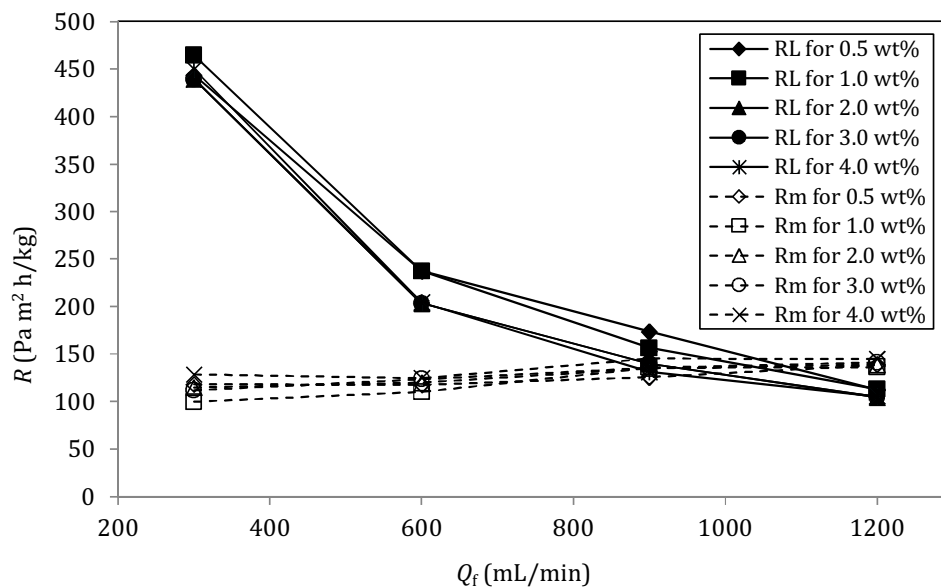
(b)

Fig. 15. Feed boundary layer resistance and membrane resistance for feed flow rates ranging from 300 to 1800 mL/min, feed temperatures ranging from 70 to 80 °C and feed concentrations ranging from 0.5 to 4.0 wt% NaCl.

rate and high feed temperature and decreased with increasing feed flow rate and decreasing feed temperature. This effect was due to the temperature polarisation effect at low feed flow rate and high feed temperature. However, the feed boundary layer resistance showed no appreciable variation with the feed concentration, e.g., 112–444 Pa m^2 h/kg at 0.5 wt% NaCl and 105–450 Pa m^2 h/kg at 4.0 wt% NaCl.

The membrane resistance increased considerably from 78–97 Pa m^2 h/kg at a feed temperature of 70 °C to 120–140 Pa m^2 h/kg at a feed temperature of 80 °C. The results indicate that the membrane resistance increased with the temperature at the membrane surface. This effect was due to the fact that the mass transfer coefficient across the membrane (C) was inversely

proportional to the temperature, as described in Eq. (4). At feed temperature of 80 °C, the membrane resistance increased slightly from 100–129 Pa m^2 h/kg at a feed flow rate of 300 mL/min to 140 Pa m^2 h/kg at a feed flow rate of 1800 mL/min. At the high feed flow rate, the temperature at the membrane surface approached the corresponding bulk temperature. The temperature at the membrane surface also increased as the bulk temperature increased. One should note that the membrane resistance slightly increased as the feed boundary layer resistance decreased. It was possible for the membrane resistance to exceed the feed boundary layer resistance at higher feed flow rates and feed temperatures. However, the membrane resistance did not change significantly with the feed concentration.

4.7. Heat transfer resistances in feed and membrane phases

The membrane may also impose significant resistance to the heat transfer process. To evaluate the heat transfer resistances in the liquid feed phase and the membrane phase, a series resistance model was employed [4,9]:

$$\frac{1}{H} = \frac{1}{h_L} + \frac{1}{h_m} \qquad (27)$$

where H and h_m are the overall heat transfer coefficient and the heat transfer coefficient of the membrane phase, respectively. The heat transfer coefficient in the membrane phase was estimated as $h_m = J\Delta H_v / \Delta T_m$ by neglecting the conductive heat lost through the membrane. The contribution of the individual heat transfer resistance was calculated as shown in Fig. 16. The data showed that up to a feed flow rate of 1200 mL/min, more than 50% of the heat transfer resistance that limited the process occurred in the feed boundary layer. Thus, the feed flow rate of 1200 mL/min was the turning point beyond which the heat transfer resistance in the membrane became dominant in the VMD process.

5. Conclusions

This work presented an experimental study of desalination via the VMD process using a rectangular cross-flow flat-sheet membrane module. The effects of the feed flow rate, feed temperature and feed concentration on the flux were investigated. The heat and mass transfer performance of the desalination via the VMD process was then evaluated. The following results were obtained:

(1) The flux increases with the flow rate of the feed solution. At higher feed flow rate, the temperature at the membrane surface approaches the corresponding temperature in the bulk phase. The dependence of the flux on the feed flow rate is reduced at relatively low feed temperatures.
(2) The flux increases exponentially with the temperature of the feed solution, as described by the Arrhenius equation. The increase in flux with temperature is attributed to the exponential increase in vapour pressure with temperature based on the Antoine equation.
(3) The flux does not change significantly with the feed concentration. The driving force of the partial pressure of
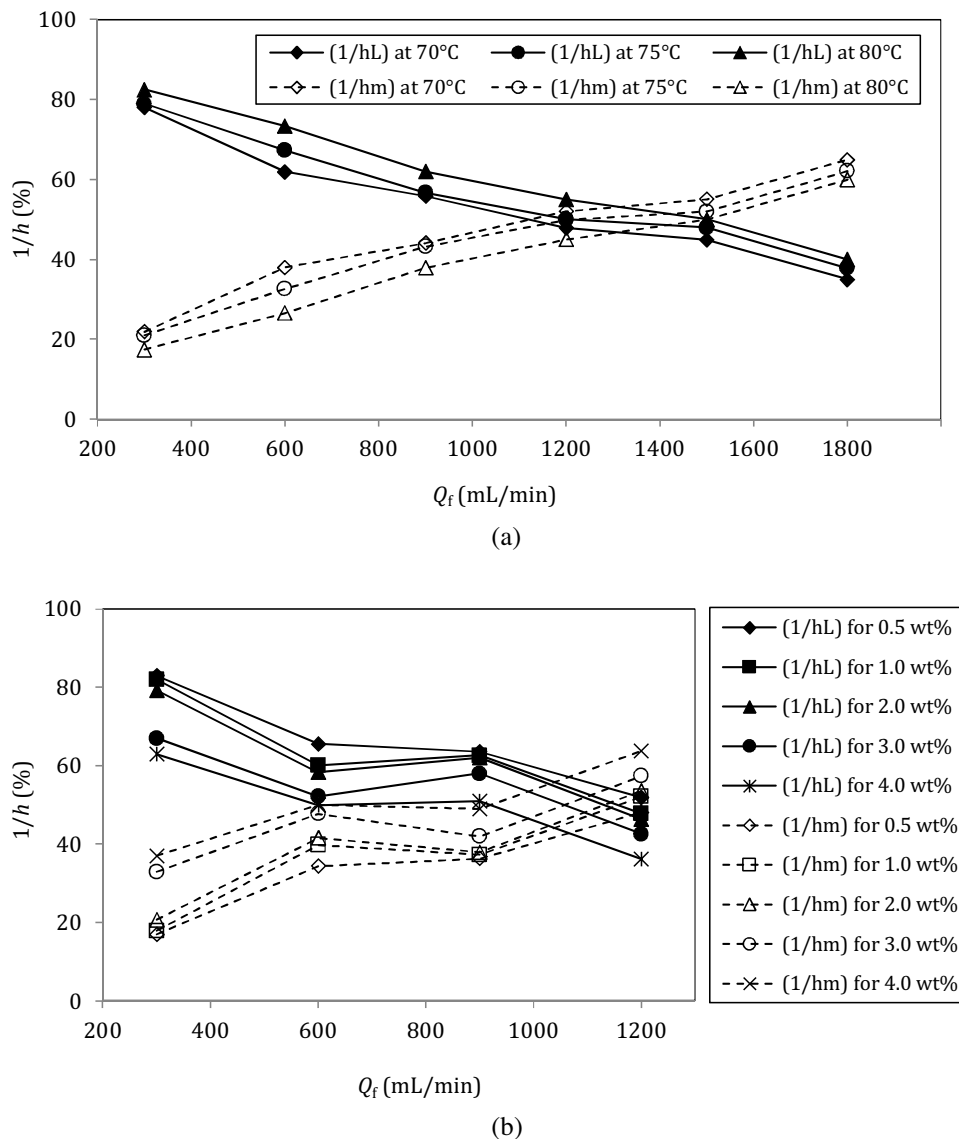
Fig. 16. Heat transfer resistances in the feed boundary layer and the membrane for feed flow rates ranging from 300 to 1800 mL/min, feed temperatures ranging from 70 to 80 °C and feed concentrations ranging from 0.5 to 4.0 wt% NaCl.

water is almost invariant over feed concentrations ranging from 0.5 to 4.0 wt% NaCl as the mole percentages and the activity coefficients of water are greater than 98.5% and 0.992, respectively.

(4) The traditional Nusselt and Sherwood correlations, which are the most common correlations employed in the MD literature, are not applicable for desalination performed using the current membrane module. However, approximately 30% of the experimental data do fit the correlations well, $Nu = aRe^b Pr^c$ and $Sh = aRe^b Sc^c$, with $a = 2.76 \times 10^{-3}$, $b = 0.97$ and $c = 3.7909$.

(5) Desalination by the VMD process is limited by the heat transferred across the feed boundary layer, whereas the mass transfer resistance in the liquid feed phase is negligible. More than 50% of the heat transfer resistances occur in the feed boundary layer when the VMD is operated at feed flow rates below 1200 mL/min, whereas the dominant heat transfer resistance occurs in the membrane itself when the flow rate exceeds 1200 mL/min. Mass transfer in the VMD process is completely controlled by the membrane itself through the Knudsen-viscous resistance.

Acknowledgements

References

[1] J.P. Mericq, S. Laborie, C. Cabassud, Evaluation of system coupling vacuum membrane distillation and solar energy for seawater desalination, Chem. Eng. J. 166 (2011) 596–606.

[2] R. Sarbatly, C.K. Chiam, Evaluation of geothermal energy in desalination by vacuum membrane distillation, Appl. Energy 112 (2013) 737–746.

[3] K. Zhao, W. Heinzl, M. Wenzel, S. Büttner, F. Bollen, G. Lange, S. Heinzl, N. Sarda, Experimental study of the memsys vacuum-multi-effect-membrane-distillation (V-MEMD) module, Desalination 323 (2013) 150–160.

[4] K.W. Lawson, D.R. Lloyd, Membrane distillation, J. Membr. Sci. 124 (1997) 1–25.

[5] A.I. Stankiewicz, J.A. Moulijn, Process intensification: transforming chemical engineering, CEP Mag. (January) (2000) 22–34.

[6] A. Alkhudhiri, N. Darwish, N. Hilal, Membrane distillation: a comprehensive review, Desalination 287 (2012) 2–18.

[7] C. Huayan, W. Chunrui, J. Yue, W. Xuan, L. Xiaolong, Comparison of three membrane distillation configurations and seawater desalination by vacuum membrane distillation, Desalin. Water Treat. 28 (2011) 321–327.

[8] S.B. Abdallah, N. Frikha, S. Gabsi, Simulation of solar vacuum membrane distillation unit, Desalination 324 (2013) 87–92.

[9] C.K. Chiam, R. Sarbatly, Vacuum membrane distillation processes for aqueous solution treatment—a review, Chem. Eng. Process. 74 (2013) 27–54.

[10] A.M. Urtiaga, G. Ruiz, I. Ortiz, Kinetic analysis of the vacuum membrane distillation of chloroform from aqueous solutions, J. Membr. Sci. 165 (2000) 99–110.

[11] M. Khayet, K.C. Khulbe, T. Matsuura, Characterisation of membranes for membrane distillation by atomic force microscopy and estimation of their water vapour transfer coefficients in vacuum membrane distillation process, J. Membr. Sci. 238 (2004) 199–211.

[12] V. Soni, J. Abildskov, G. Jonsson, R. Gani, Modelling and analysis of vacuum membrane distillation for the recovery of volatile aroma compounds from black currant juice, J. Membr. Sci. 320 (2008) 442–455.

[13] K.W. Lawson, D.R. Lloyd, Membrane distillation. I. Module design and performance evaluation using vacuum membrane distillation, J. Membr. Sci. 120 (1996) 111–121.

[14] J.I. Mengual, M. Khayet, M.P. Godino, Heat and mass transfer in vacuum membrane distillation, Int. J. Heat Mass Transfer 47 (2004) 865–875.

[15] B. Qi, B. Li, S. Wang, Investigation of shell side heat transfer in cross-flow designed vacuum membrane distillation module, Ind. Eng. Chem. Res. 51 (2012) 11463–11472.

[16] C.K. Chiam, R. Sarbatly, Heat transfer in the rectangular cross-flow flat-sheet membrane module for vacuum membrane distillation, Chem. Eng. Process. 79 (2014) 23–33.

[17] M. Khayet, Membranes and theoretical modelling of membrane distillation: a review, Adv. Colloid Interface Sci. 164 (2011) 56–88.

[18] S.G. Lovineh, M. Asghari, B. Rajaei, Numerical simulation and theoretical study on simultaneous effects of operating parameters in vacuum membrane distillation, Desalination 314 (2013) 59–66.

[19] J. Zhang, J.D. Li, M. Duke, M. Hoang, Z. Xie, A. Groth, C. Tun, S. Gray, Modelling of vacuum membrane distillation, J. Membr. Sci. 434 (2013) 1–9.

[20] S.M. Shim, J.G. Lee, W.S. Kim, Performance simulation of a multi-VMD desalination process including the recycle flow, Desalination 338 (2014) 39–48.

[21] H. Fan, Y. Peng, Application of PVDF membranes in desalination and comparison of the VMD and DCMD processes, Chem. Eng. Sci. 79 (2012) 94–102.

[22] J.M. Smith, H.C. Van Ness, M.M. Abbott, Chemical Engineering Thermodynamics, six ed., McGraw-Hill, New York, 2001.

[23] Z.P. Zhao, C.Y. Zhu, D.Z. Liu, W.F. Liu, Concentration of ginseng extracts aqueous solution by vacuum membrane distillation 2. Theory analysis of critical operating conditions and experimental confirmation, Desalination 267 (2011) 147–153.

[24] M. Gryta, Concentration of NaCl solution by membrane distillation integrated with crystallisation, Sep. Sci. Technol. 37 (2002) 3535–3558.

[25] B. Li, K.K. Sirkar, Novel membrane and device for vacuum membrane distillation-based desalination process, J. Membr. Sci. 257 (2005) 60–75.

[26] J.G. Lee, W.S. Kim, Numerical study on multi-stage vacuum membrane distillation with economic evaluation, Desalination 339 (2014) 54–67.

[27] N. Couffin, C. Cabassud, V. Lahoussine-Turcaud, A new process to remove halogenated VOCs for drinking water production: vacuum membrane distillation, Desalination 11 (1998) 233–245.

[28] A.C. Sun, W. Kosar, Y. Zhang, X. Feng, Vacuum membrane distillation for desalination of water using hollow fibre membranes, J. Membr. Sci. 455 (2014) 131–142.

[29] M.S. El-Bourawi, Z. Ding, R. Ma, M. Khayet, A framework for better understanding membrane distillation separation process, J. Membr. Sci. 285 (2006) 4–29.

[30] S. Srisurichan, R. Jiraratananon, A.G. Fane, Mass transfer mechanisms and transport resistances in direct contact membrane distillation process, J. Memr. Sci. 277 (2006) 186–194.

[31] S. Bandini, C. Gostoli, G.C. Sarti, Separation efficiency in vacuum membrane distillation, J. Membr. Sci. 73 (1992) 217–229.

[32] L. Martínez, F.J. Florido-Díaz, Theoretical and experimental studies on desalination using membrane distillation, Desalination 139 (2001) 373–379.

[33] J. Phattaranawik, R. Jiraratananon, A.G. Fane, C. Halim, Mass flux enhancement using spacer filled channels in direct contact membrane distillation, J. Membr. Sci. 187 (2001) 193–201.

[34] Y. Yun, R. Ma, W. Zhang, A.G. Fane, J. Li, Direct contact membrane distillation mechanism for high concentration NaCl solutions, Desalination 188 (2006) 251–262.

[35] X. Wang, L. Zhang, H. Yang, H. Chen, Feasibility research of potable water production via solar-heated hollow fibre membrane distillation system, Desalination 247 (2009) 403–411.

[36] S. Kimura, S.I. Nakao, S.I. Shimatani, Transport phenomena in membrane distillation, J. Membr. Sci. 33 (1987) 285–298.

[37] M. Gryta, M. Tomaszewska, Heat transport in the membrane distillation process, J. Membr. Sci. 144 (1998) 211–222.

[38] J. Phattaranawik, R. Jiraratananon, A.G. Fane, Heat transport and membrane distillation coefficients in direct contact membrane distillation, J. Membr. Sci. 212 (2003) 177–193.

[39] M. Gryta, M. Tomaszewska, A.W. Morawski, Membrane distillation with laminar flow, Sep. Purif. Technol. 11 (1997) 93–101.

[40] M. Tomaszewska, M. Gryta, A.W. Morawski, Mass transfer of HCl and H_2O across the hydrophobic membrane during membrane distillation, J. Membr. Sci. 166 (2000) 149–157.

[41] R.W. Schofield, A.G. Fane, C.J.D. Fell, R. Macoun, Factors affecting flux in membrane distillation, Desalination 77 (1990) 279–294.

[42] C.J. Geankoplis, Transport Processes and Separation Process Principles, fourth ed., Prentice Hall, New Jersey, 2003.

[43] S. Bandini, A. Saavedra, G.C. Sarti, Vacuum membrane distillation: experiments and modelling, AIChE J. 43 (1997) 398–408.

[44] D. Wirth, C. Cabassud, Water desalination using membrane distillation: comparison between inside/out and outside/in permeation, Desalination 147 (2002) 130–145.

[45] F.A. Banat, J. Simandl, Removal of benzene traces from contaminated water by vacuum membrane distillation, Chem. Eng. Sci. 51 (1996) 1257–1265.

[46] M.S. El-Bourawi, M. Khayet, R. Ma, Z. Ding, Z. Li, X. Zhang, Application of vacuum membrane distillation for ammonia removal, J. Membr. Sci. 301 (2007) 200–2009.